MoBiFC: development of a modular bimolecular fluorescence complementation toolkit for the analysis of chloroplast protein-protein interactions

Florent Velay, Melanie Soula, Marwa Mehrez, Stefano d'Alessandro, Christophe Laloi, Patrice Crete, Ben Field, Clément Belbachir

Velay *et al. Plant Methods* (2022) 18:69
https://doi.org/10.1186/s13007-022-00902-1

Plant Methods

METHODOLOGY

Open Access

MoBiFC: development of a modular bimolecular fluorescence complementation toolkit for the analysis of chloroplast protein–protein interactions

Florent Velay[1], Mélanie Soula[1], Marwa Mehrez[1,2], Clément Belbachir[1], Stefano D'Alessandro[1,3], Christophe Laloi[1], Patrice Crete[1*] and Ben Field[1*]

Abstract

Background: The bimolecular fluorescence complementation (BiFC) assay has emerged as one of the most popular methods for analysing protein–protein interactions (PPIs) in plant biology. This includes its increasing use as a tool for dissecting the molecular mechanisms of chloroplast function. However, the construction of chloroplast fusion proteins for BiFC can be difficult, and the availability and selection of appropriate controls is not trivial. Furthermore, the challenges of performing BiFC in restricted cellular compartments has not been specifically addressed.

Results: Here we describe the development of a flexible modular cloning-based toolkit for BiFC (MoBiFC) and proximity labelling in the chloroplast and other cellular compartments using synthetic biology principles. We used pairs of chloroplast proteins previously shown to interact (HSP21/HSP21 and HSP21/PTAC5) and a negative control (HSP21/ΔPTAC5) to develop standardised Goldengate-compatible modules for the assembly of protein fusions with fluorescent protein (FP) fragments for BiFC expressed from a single multigenic T-DNA. Using synthetic biology principles and transient expression in *Nicotiana benthamiana*, we iteratively improved the approach by testing different FP fragments, promoters, reference FPs for ratiometric quantification, and cell types. A generic negative control (mCHERRY) was also tested, and modules for the identification of proximal proteins by Turbo-ID labelling were developed and validated.

Conclusions: MoBiFC facilitates the cloning process for organelle-targeted proteins, allows robust ratiometric quantification, and makes available model positive and negative controls. Development of MoBiFC underlines how Goldengate cloning approaches accelerate the development and enrichment of new toolsets, and highlights several potential pitfalls in designing BiFC experiments including the choice of FP split, negative controls, cell type, and reference FP. We discuss how MoBiFC could be further improved and extended to other compartments of the plant cell and to high throughput cloning approaches.

Keywords: Bimolecular fluorescence complementation, Protein interactions, Chloroplast

Background

The characterisation of protein protein interactions (PPIs) is important for understanding the assembly of macromolecular machines and deciphering the signal transduction pathways that are required for regulating

*Correspondence: patrice.crete@univ-amu.fr; ben.field@univ-amu.fr

[1] Aix-Marseille Univ, CEA, CNRS, BIAM, UMR7265, 13009 Marseille, France
Full list of author information is available at the end of the article

the growth, development, and acclimation of plants in a constantly changing environment. A wide range of orthogonal methods are used to study PPIs, including yeast two-hybrid, affinity purification, and protein-fragment complementation assays [21, 44]. The bimolecular fluorescence complementation (BiFC) or split-fluorescent protein (FP) assay has emerged as the most popular protein-fragment complementation method in plant biology [19, 29, 44]. BiFC relies on assembly of a stable FP upon the interaction between two proteins of interest (POIs) each fused to separate non-fluorescent fragments of the FP [34]. The popularity and power of BiFC lies in its relative simplicity, in vivo nature, and ability to capture weak or transient PPIs. The first BiFC assay was performed using a GFP split in mammalian cells [15]. Subsequently, many different splits and GFP variants were developed with the aim of improving signal strength and reducing non-specific complex assembly [19, 44]. Further innovations followed, including the development of vector systems allowing the co-expression of the POIs and reference FPs from the same construction [9, 10], the use of super-resolution compatible FPs, and multicolour or trimolecular complementation assays that allow the simultaneous visualization of multiple protein complexes [44]. While BiFC is an attractive and powerful technique that is often used in combination with yeast two-hybrid and affinity purification, the stable nature of the assembled FP means that particular attention must be paid to the selection of appropriate controls to avoid false positives [9, 14, 18, 19]. Kudla and Bock [19] advise that the most appropriate negative control is a BiFC assay using a mutated POI lacking its interaction domain or a member of the same protein family that does not interact with the partner protein.

In plants there are reports of successful BiFC assays in multiple cellular compartments, including the cytosol, nucleus [3], chloroplast [5, 26], and more recently in the mitochondria [43, 52]. However, despite the growing number of studies reporting organellar PPIs by BiFC only a handful use gold-standard negative controls [13, 27, 30, 33, 46, 49] and many fall far short. For example, a surprising number of studies lack any negative control, or use the expression of a cytosolic FP fragment as a negative control for the interaction between chloroplastic POIs. In the latter case, the negative control is unlikely to be sufficient alone to detect non-specific assembly because, without a chloroplast transit peptide, the free FP fragment cannot encounter the POI in the chloroplast. In addition, no study has specifically addressed whether the small volume of compartments in the chloroplasts and mitochondria can affect the outcomes of BiFC assays. Indeed, because BiFC fusion proteins are usually highly expressed, their concentration in restricted cellular compartments will increase the frequency of random protein–protein collisions and could lead to false positive BiFC signals.

Adding to these difficulties, the study of organellar PPIs by BiFC and other techniques is also hindered by the presence of targeting peptides. The position of the FP fragment fusion at the N or C terminus of a POI can affect the ability of the POI to interact with partner proteins [29]. Therefore, it is common to test all FP fusions orientations in all possible combinations with the target protein to maximize the chances of identifying a PPI. However, transit peptides complicate the cloning process for FP fusions. It is likely for this reason that, to our knowledge, the great majority of BiFC experiments carried out in the chloroplasts and mitochondria to date involve POIs with C-terminus FP fragment fusions.

To further explore and overcome the challenges associated with performing organellar BiFC we developed a modular approach based on Modular Cloning (MoClo) [6, 7, 51]. The modular nature of the approach simplifies cloning of chloroplast proteins, and allows the assembly of all transcriptional units including a reference protein on a single construct. Using synthetic biology principles, we designed, built and tested components to arrive at an optimised system suitable for testing protein–protein interactions in the chloroplast by quantitative BiFC. Development of the system highlighted a number of factors critical for performing successful chloroplastic BiFC including the selection of negative controls, the nature of the FP split used, the cell type analysed, and the choice of reference protein for quantification. Finally, we discuss how the MoClo-based BiFC approach could be extended to other organelles and adapted to other interaction methods.

Results

A modular system for testing interactions by BiFC

The MoClo cloning system provides an attractive framework for the assembly and in planta expression of chimeric proteins. Using the MoClo syntax we conceived an approach for the systematic assembly of gene fusions for BiFC that we named MoClo-based BiFC or MoBiFC (Fig. 1). In MoBiFC, the coding sequence (CDS) of an FP fragment is fused upstream or downstream to the CDS of a protein of interest (POI). A generic targeting presequence (e.g., encoding a chloroplast transit peptide) can be included. A second synthetic gene encoding the interaction partner to be tested is assembled in the same way with the complementary FP fragment, and the two genes are then assembled in a multigenic T-DNA along with a gene encoding the suppressor of silencing P19 [41] and a fluorescent marker of transformation (Fig. 1C).

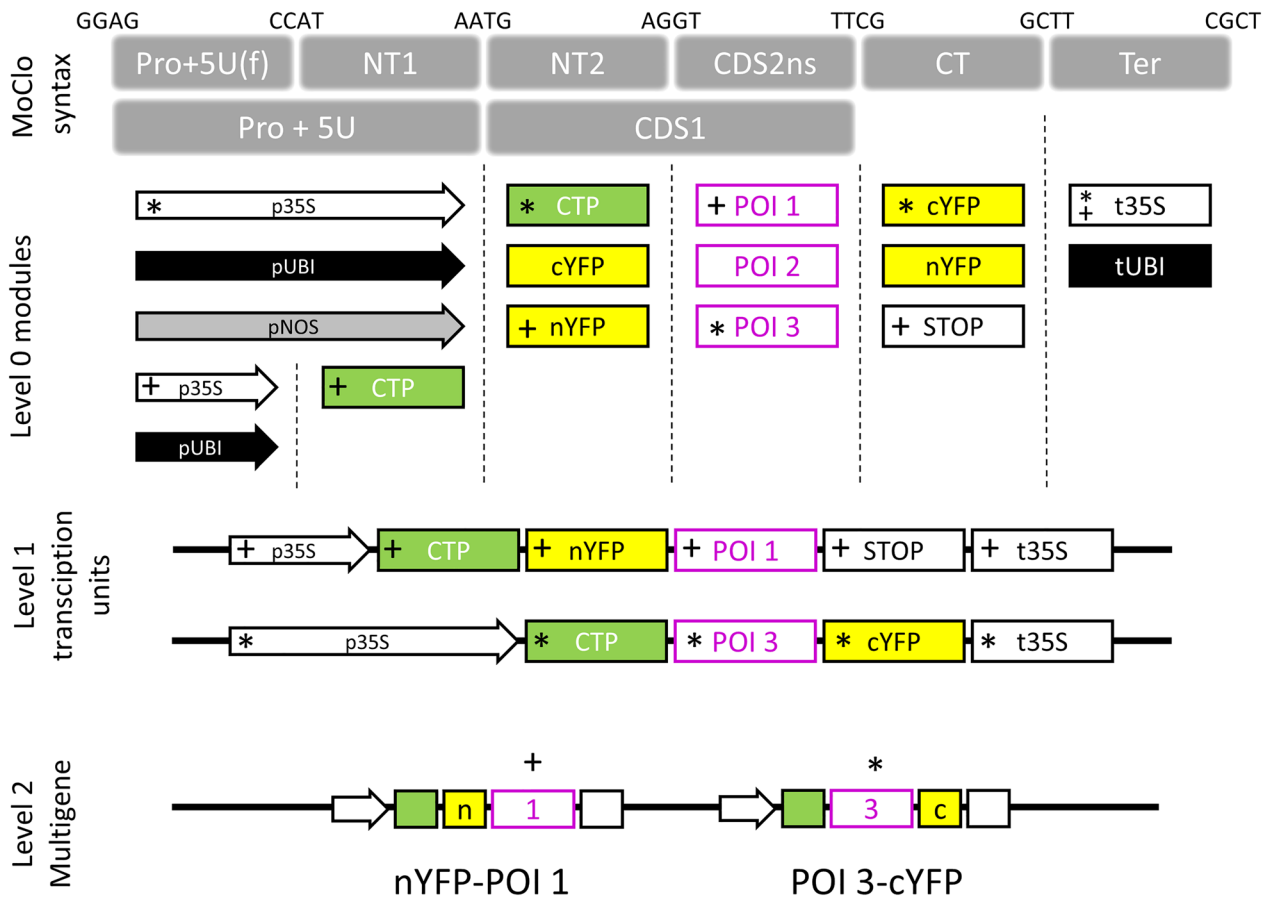

Fig. 1 Outline of a MoClo-based approach for testing protein–protein interactions by BiFC. The MoClo syntax for the position of different modules is indicated on the top line, and is as described by Engler et al. [6]. Level 0 modules containing promoter and 5′ UTR sequences [Pro + 5U(f), Pro + 5U], N-terminal targeting sequences and tags (NT1, NT2), coding sequences for a protein of interest (CDS2ns), C-terminal tags (CT) and transcription terminators (Ter) are assembled in a one-pot restriction ligation reaction into Level 1 transcriptional units using the indicated four base-pair overhangs. The transcriptional units are then assembled in a similar fashion into single T-DNA Level 2 multigenic assemblies for BiFC assays. As an example, + and * indicate Level 0 modules selected for creating the shown Level 1 transcriptional units, that are then assembled into a Level 2 multigenic array. p35S, cauliflower mosaic virus 35S promoter; pUBI, *UBQ10* promoter; CTP, chloroplast transit peptide; cYFP, C-terminal fragment of YFP for BiFC; nYFP, N-terminal fragment of YFP for BiFC; POI, protein of interest without transit peptide or stop codon; STOP, module containing a stop codon; t35S, cauliflower mosaic virus 35S terminator; tUBI, UBQ10 terminator

As proof of principle we tested the chloroplast protein HSP21 that is known to interact with itself [20, 35, 54]. We assembled synthetic fusion genes using the mature HSP21 CDS (i.e., the native chloroplast transit peptide was removed), the two fragments of the 174/175 YFP split [5] and the Rubisco small subunit transit peptide (CTP-SSU) for chloroplast targeting [22]. YFP fluorescence was observed in the chloroplasts of *Nicotiana benthamiana* leaf mesophyll cells, indicating re-assembly of YFP due to the interaction between HSP21-nYFP and HSP21-cYFP (Additional file 1: Fig. S1A). The signal showed the same pattern as HSP21-GFP (Additional file 1: Fig. S1B), and was similar to the BiFC pattern reported previously for HSP21 [54]. Next, to enable detection of fusion proteins by immunoblot, we added a triple FLAG tag to the N-terminal fragment of YFP and a triple HA tag to the C-terminal fragment. When tested with HSP21 the tagged and untagged versions of the YFP fragments displayed a comparable interaction signal in terms of fluorescence intensity and localisation, indicating that the presence of the epitope tags does not disturb the BiFC (Additional file 1: Fig. S1A). The epitope tags were also easily detectable by immunoblotting (Additional file 1: Fig. S1C). We will refer to 3FLAG_nYFP and cYFP_3HA as nYFP and cYFP from here onwards. These experiments indicate that the new MoClo components are functional, and that the MoClo system is suitable for assembling gene fusions for performing chloroplastic BiFC.

MoBiFC can be used to robustly test protein–protein interactions in the chloroplast

Next, we tested the BiFC system using different partner proteins and controls. We first selected the pair HSP21 and PTAC5 that were previously shown to interact by BiFC and pull-down assays [54]. We found that expression of HSP21-nYFP and PTAC5-cYFP resulted in reconstitution of YFP fluorescence in a similar pattern to HSP21-nYFP/HSP21-cYFP in the mesophyll cells (Fig. 2A, B). The nucleo-cytoplasmic CFP served as a useful transformation control, allowing the identification of cells containing the multigenic T-DNA. Zhong et al. [54] showed that deletion of a C-terminal region (253–387) of PTAC5 abolished the HSP21-PTAC5 interaction. We therefore tested the interaction of HSP21 with PTAC5 lacking this C-terminal region (ΔPTAC5) to determine whether it acted as a suitable negative control. We observed a significant drop in fluorescence intensity compared to HSP21-nYFP/PTAC5-cYFP, although we were still able to detect YFP reconstitution in a similar speckled pattern (Fig. 2B, Additional file 1: Fig. S2A, B). While our results confirm ΔPTAC5 as a suitable negative control for PTAC5, no speckles were reported for HSP21-nYFP/ΔPTAC5-cYFP in the previous study [54]. This may be due to differences in experimental setup (*N. benthamiana*

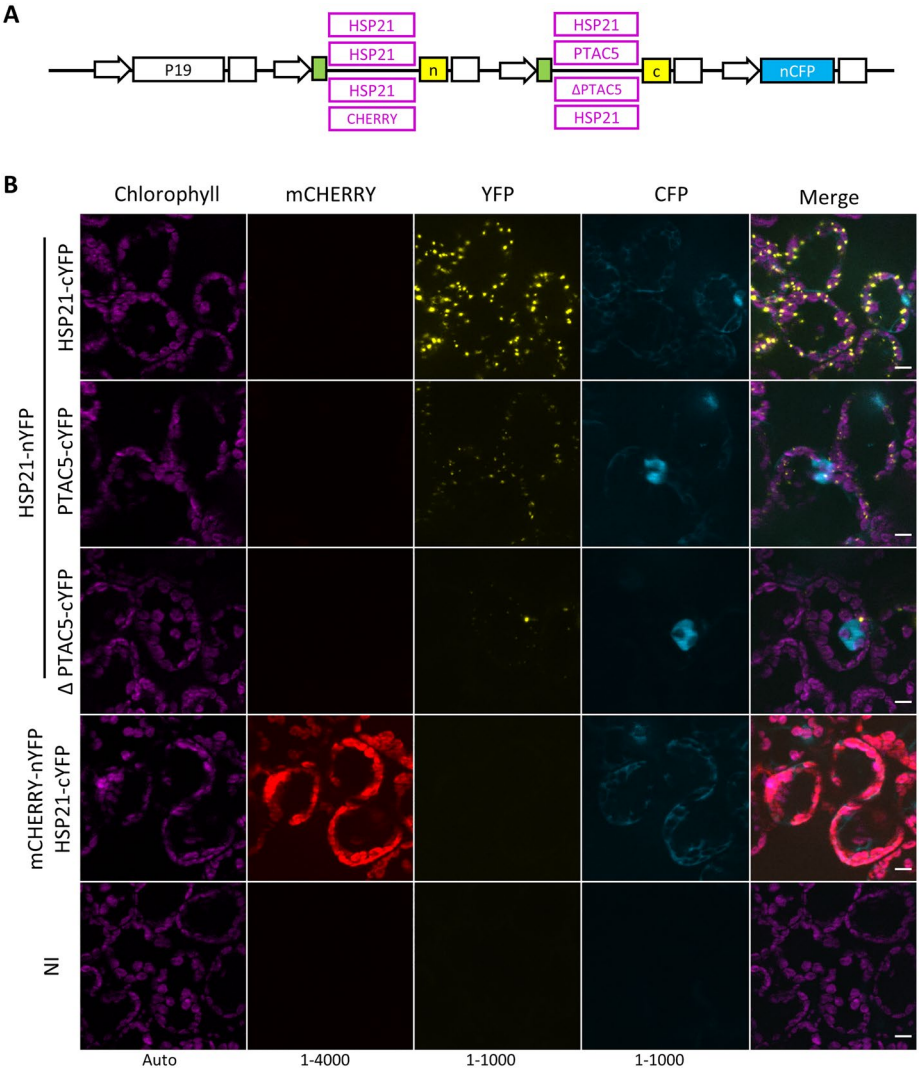

Fig. 2 mCHERRY-nYFP and HSP21-cYFP do not produce a non-specific assembly signal in the chloroplast. **A** The POI region of the multigenic BiFC construction was varied to produce four different chloroplast targeted HSP21 pairs that were used for **B** BiFC assays in *N. benthamiana* mesophyll cells. NI, not inoculated; n, nYFP; c, cYFP; scale, 10 µm; histogram levels shown at the bottom of each channel. Modules and plasmids are described in Additional file 2: Table S1 and full plasmid sequences are available in Additional file 4

mesophyll cells here versus Arabidopsis protoplasts previously) or post acquisition analysis.

We next searched for a negative control with the potential to be used in a more general fashion. We selected the monomeric fluorescent protein mCHERRY as a candidate [42]. Chloroplast-targeted mCHERRY-nYFP showed strong mCHERRY fluorescence in the chloroplasts, and a very low BiFC signal in the presence of HSP21-cYFP expressed from the same T-DNA. The mCHERRY BiFC signal showed no speckles, and was significantly lower than the HSP21-nYFP/HSP21-cYFP signal (Additional file 1: Fig. S2A). Surprisingly, mCHERRY-nYFP/HSP21-cYFP showed a higher signal than HSP21-nYFP/ΔPTAC-cYFP, despite the presence of visible speckles for the second pair. These differences in signal are likely due to differences in protein localisation and abundance, and highlight the importance of these factors in making comparisons between BiFC pairs. Together, these results indicate that mCHERRY can act as a useful generic negative control for BiFC. mCHERRY has the advantage of showing a homogenous stroma localisation, and fluorescence that can be visualised directly during microscopy to allow rapid assessment of BiFC interaction specificity.

MoBiFC allows N-terminal fusion proteins to be tested within the chloroplast

The MoBiFC cloning approach allows the straightforward introduction of an N-terminal tag between a generic chloroplast transit peptide (the Rubisco small subunit CTP) and the POI (Fig. 1). To test whether BiFC is still functional in this configuration we performed BiFC assays with the YFP fragments fused to the N-terminal of the proteins of interest (Fig. 3A). N-terminal tagged HSP21 showed a similar BiFC signal to C-terminal tagged HSP21 (Fig. 3B), indicating that chloroplast import, HSP21/HSP21 interaction and YFP reconstitution are not hindered. Therefore, the MoClo based BiFC approach allows the straightforward generation of N- and C-terminal tagged protein fusions for chloroplastic BiFC assays.

Optimisation of MoBiFC with different promoters, FP splits and reference FPs

The modular nature of the MoClo system allows different components to be swapped in and tested. We therefore sought to determine whether altering the fluorescent protein split or promoters could improve performance using the HSP21 pair (Fig. 4A). We first replaced the 174/175 YFP split with the 210/211 mVENUS split that was reported to display a lower level of non-specific assembly [9]. The HSP21-nVENUS/HSP21-cVENUS interaction pattern was very similar to the YFP split, while the strength of the fluorescence signal doubled and nVENUS fusion protein accumulation also increased (Fig. 4B, Additional file 1: Fig. S3A, B). However, the mCHERRY-nVENUS/HSP21-cVENUS negative control produced almost 4 times higher non-specific signal than for the corresponding YFP split (Additional file 1: Fig. S3A). A possible explanation for the higher non-specific signal is self-complementation within the mCHERRY-nVENUS fusion protein, or fluorescence bleed-through from mCHERRY into the YFP channel. However, we did not detect significant bleed through, and found that the non-specific signal was detectable only when mCHERRY-nVENUS was expressed with HSP21-cVENUS (Additional file 1: Fig. S4). Therefore, the mVENUS split increases the BiFC signal intensity, but this can be accompanied by an increase in non-specific assembly in at least some cases.

The strong 35S promoter of the cauliflower mosaic virus was used to drive expression of the fusion genes in the previous experiments. High expression levels could be responsible for driving non-specific assembly of the mVENUS split. We therefore attempted to reduce expression levels to improve the signal to noise ratio. For this purpose, we used the Arabidopsis *UBQ10* promoter which was shown to be substantially weaker than the 35S promoter in tobacco [11]. While the fluorescence intensity was somewhat reduced for the HSP21/HSP21 pair we still observed the diffuse mVENUS signal in the mCHERRY/HSP21 negative control (Fig. 4B, Additional file 1: Fig. S3B). Along with the reduction in fluorescence, immunoblotting showed a small but clear decrease in levels of fusion proteins produced using the *UBQ10* promoter (Additional file 1: Fig. S3C). Taken together, our attempts at optimisation indicate that the 35S promoter and the 174/175 YFP split modules are currently the best choice for BiFC in the chloroplast under these conditions.

We next turned to the reference FP. While useful, the nucleo-cytosolic CFP shows a rather weak fluorescence and is sometimes difficult to find in mesophyll cells. The signal is also not proportional to chloroplast area within a region of interest, so is not suitable for ratiometric BiFC quantification despite its presence on the same T-DNA. We therefore swapped out the nucleo-cytosolic CFP from the BiFC T-DNA and replaced it with either chloroplast targeted CFP (CTP-CFP) or an OEP7 monomeric Turquoise (mTRQ) fusion (OEP7-mTRQ) (Fig. 5A, Additional file 1: Fig. S5A). OEP7 is a protein of the chloroplast outer envelope membrane, and OEP7-GFP was previously used as an outer envelope membrane marker [23]. mTRQ is a monomeric variant of CFP with a higher quantum yield [7, 8, 12]. Both CTP-CFP and OEP7-mTRQ clearly marked the chloroplasts in transformed cells of the epidermis and mesophyll and showed a more intense fluorescence than the nucleo-cytosolic

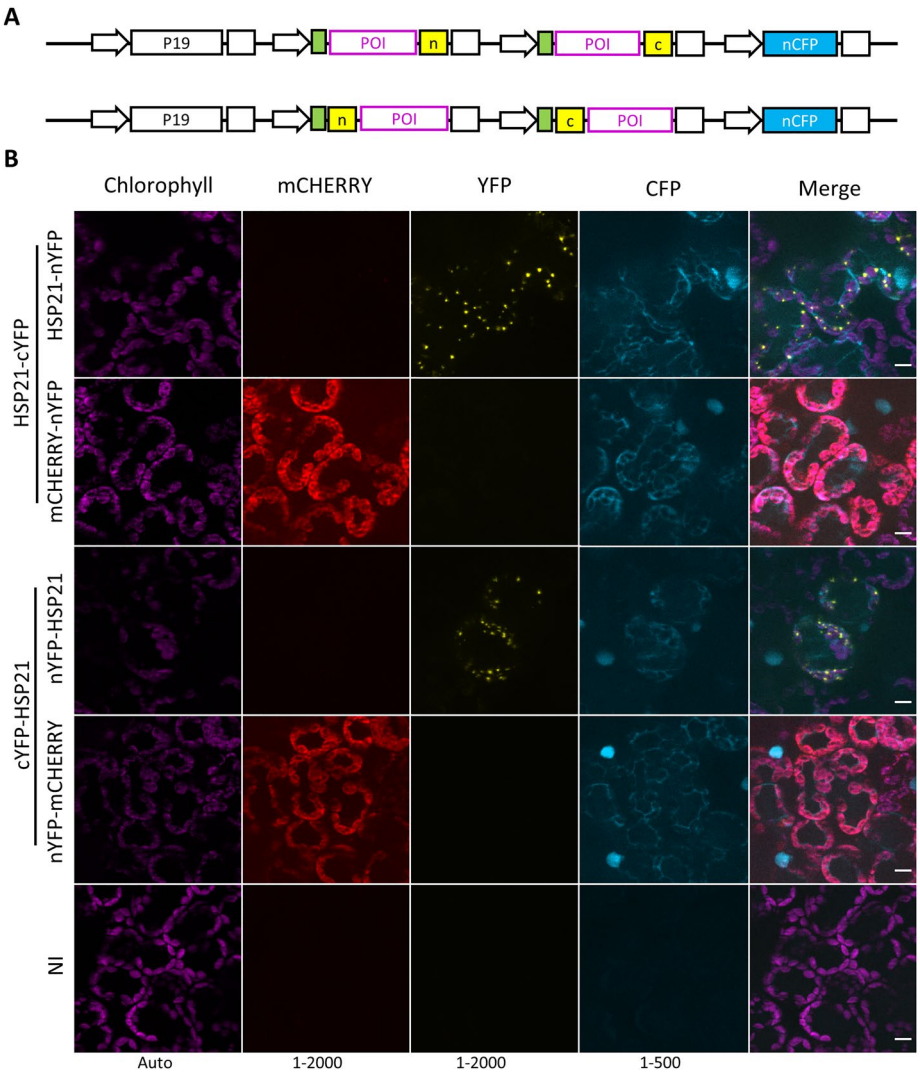

Fig. 3 N-terminal FP fusions function similarly to C-terminal fusions in BiFC experiments. **A** Chloroplast targeted HSP21 and HSP21/mCHERRY pairs with C-terminal and N-terminal FP fragment fusions were used for **B** BiFC assays in *N. benthamiana* mesophyll cells. NI, not inoculated; n, nYFP; c, cYFP; scale, 10 µm; histogram levels shown at the bottom of each channel. Modules and plasmids are described in Additional file 2: Table S1 and full plasmid sequences are available in Additional file 4

CFP (Fig. 5B, Additional file 1: Fig. S5B). The signal for the HSP21-nYFP/HSP21-cYFP interaction in the chloroplasts was also preserved. However, cells transformed with CTP-CFP regularly showed mCHERRY and YFP signals in the cytosol (Additional file 1: Fig. S5B). This indicates that co-expression of CTP-CFP interferes with the chloroplast localisation of HSP21 and mCHERRY chloroplast. The integrity of the chloroplasts did not appear to be affected, suggesting that the mis-localisation may therefore be linked to saturation of the chloroplast import machinery. In contrast, we never observed cytosolic mCHERRY or YFP signals in mesophyll cells co-expressing OEP7-mTRQ. OEP7 insertion in the chloroplast membrane does not compete with Rubisco SSU import and is independent of known chloroplast translocons [36, 39]. Therefore, it is likely that the use of OEP7-mTRQ prevents the saturation of the chloroplast import machinery that appears to occur when multiple chloroplast targeted proteins are co-expressed at high levels. Importantly, we also found that OEP7-mTRQ fluorescence was proportional to mCHERRY-nYFP fluorescence, which varies between cells Fig. 5B). The proportional accumulation of OEP7-mTRQ combined with its neutral chloroplast localisation therefore allows accurate ratiometric quantification of specific and non-specific chloroplast based BiFC signals (Fig. 5C). We next

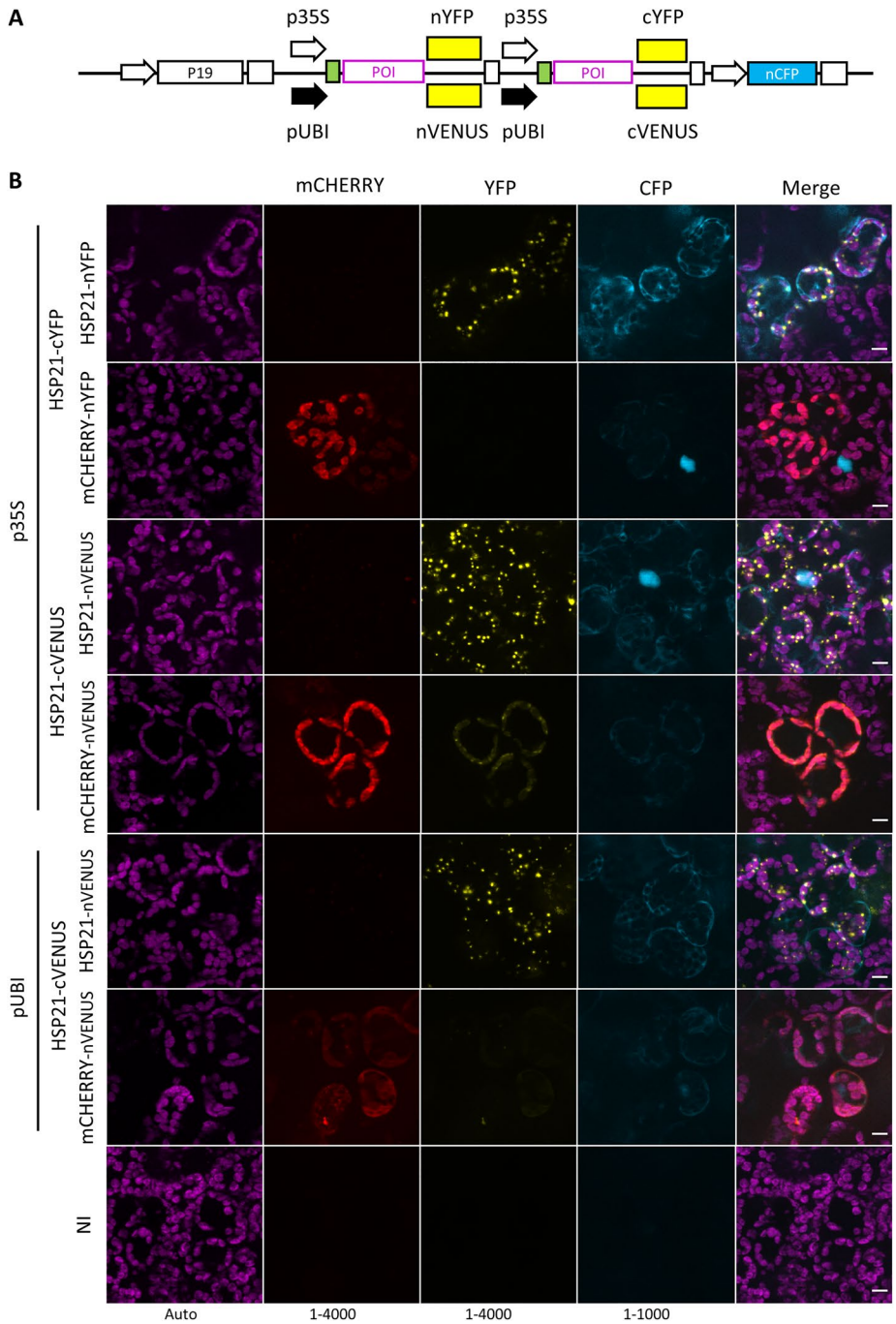

Fig. 4 The sensitivity of the BiFC can be adjusted with different FP splits and promoters. **A** The promoter and FP fragment regions in the multigenic BiFC construct were varied to produce six different chloroplast targeted HSP21 pairs that were used for **B** BiFC assays in *N. benthamiana* mesophyll cells. NI, not inoculated. Scale, 10 µm; histogram levels shown at the bottom of each channel. Modules and plasmids are described in Additional file 2: Table S1 and full plasmid sequences are available in Additional file 4

tested whether OEP7-mTRQ accumulation was affected when incorporated in different multigenic BiFC T-DNAs (HSP21-nYFP/HSP21-cYFP and the mCHERRY-nYFP/HSP21-cYFP). Unexpectedly, OEP7-mTRQ levels where lower when co-expressed with HSP21-nYFP than mCHERRY-nYFP (Additional file 1: Fig. S8A). Nevertheless, HSP21-nYFP levels were also lower, resulting in the same expression ratio in the two contexts (Additional

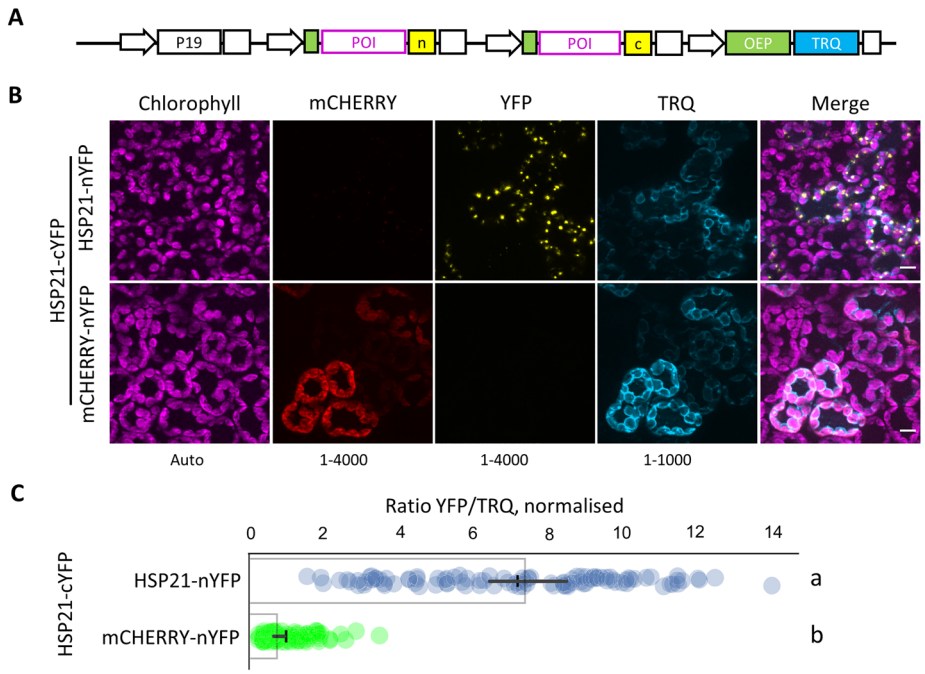

Fig. 5 OEP7-mTRQ is a suitable reference FP for ratiometric chloroplastic BiFC. **A** Outline of multigenic BiFC construct encoding an OEP7-mTRQ reference FP that was used for **B** BiFC assays between two protein pairs in *N. benthamiana* mesophyll cells. Scale, 10 µm; histogram levels shown at the bottom of each channel. **C** Normalised BiFC signals were calculated as the ratio between total YFP and TRQ fluorescence. The negative control (HSP21-cYFP/mCHERRY-nYFP) was set to 1. Bar indicates mean and cross indicates median ± 95% confidence interval (n = 100 transformed cells). Significance was calculated using the Kruskal Wallis test, groups are indicated by lower case letters ($P < 0.001$). n, nYFP; c, cYFP. Modules and plasmids are described in Additional file 2: Table S1 and full plasmid sequences are available in Additional file 4

file 1: Fig. S8B). Care must therefore be taken when setting up ratiometric BiFC experiments to avoid bias that might arise from context dependent changes in expression of the reporter.

Non-specific assembly in different *N. benthamiana* cell types

During the numerous experiments carried out in *N. benthamiana*, we noticed that different tissues did not show the same response in the BiFC assays. Mesophyll cells from the upper and lower side of the leaf always showed comparable results. However, epidermal cells often showed BiFC signals for the HSP21-nYFP/HSP21-cYFP pair that were much stronger and differently distributed than those observed in the mesophyll (Additional file 1: Fig. S6). Furthermore, the negative control mCHERRY-nYFP/HSP21-cYFP showed a non-specific BiFC signal. Interestingly, BiFC assays in Arabidopsis epidermal cells using the same constructions showed a specific and correctly localised HSP21-nYFP/HSP21-cYFP interaction without non-specific mCHERRY-nYFP/HSP21-cYFP assembly (Additional file 1: Fig. S7). However, the signal intensity in Arabidopsis was considerably lower than in *N. benthamiana* epidermal cells. Taken together, these observations might therefore suggest that the combination of high expression levels in *N. benthamiana* and the small size of epidermal chloroplasts can lead to protein overaccumulation within the chloroplasts. High protein concentrations will favour the spontaneous self-assembly of the YFP split and will also increase the formation of protein aggregates with incorrect localisation.

MoBiFC modules can be rapidly adapted for other approaches

The universal MoClo assembly syntax allows the re-use of Level 0 modules for other applications. BiFC is mostly performed using two known POIs, and candidate POIs must first be identified using other methods such as co-immunoprecipitation followed by mass spectrometry (MS). PPI identification has recently received a boost thanks to new proximity labelling approaches such as the use of the optimised promiscuous biotin ligase TurboID that, when fused to a POI, biotinylates proteins within the immediate vicinity [4]. Proteins biotinylated by the POI-TurboID fusion can then be isolated and identified by MS. Several studies now show that TurboID functions well for PPI identification in plants, and is even able to

identify transient interactions such as those between a kinase and its substrate [1, 17, 25, 53]. However, to our knowledge TurboID or any other proximity labelling method have not yet been demonstrated in the chloroplast. We therefore designed TurboID modules in the MoClo syntax for N and C-ter fusions to chloroplast targeted POIs (Additional file 1: Fig. S9A). A chloroplast targeted YFP-TurboID fusion localises correctly to the chloroplast where it biotinylates a range of proteins including a co-expressed chloroplast targeted CFP (Additional file 1: Fig. S9B, C). While this experiment shows that TurboID is functional within the chloroplast, it also highlights the promiscuous nature of TurboID. For the identification of genuine interactors a non-interacting TurboID control will therefore be required to allow the quantitative demonstration that a POI preferentially labels a specific subset of chloroplast proteins. This addition to the toolkit will complement the BiFC tools by facilitating the de novo identification of POIs within the chloroplast and other cellular compartments.

Conclusions

We describe the development of a new BiFC approach and toolkit for the investigation of protein–protein interactions in the chloroplast. The approach facilitates the cloning process for chloroplast-targeted proteins, allows robust ratiometric quantification, and the toolkit comes with model positive and negative controls for chloroplastic BiFC (Fig. 6, Additional file 2: Table S1). Furthermore, the open design of MoClo based systems facilitates user-driven optimisation and enrichment with new modules and functions. As an example, we demonstrate a complementary MoClo TurboID module that could be further developed for the identification of candidate interactors by proximity labelling in the chloroplast or other compartments of the cell. Our study also highlighted the pitfalls that can occur in setting up chloroplastic BiFC assays. We find that the choice of FP split, negative controls, cell type, reference FP localisation and expression levels can have major effects on the outcome of a BiFC experiment.

We show that chloroplast targeted mCHERRY is a useful generic negative control for chloroplast BiFC assays due to its intrinsic fluorescence and homogenous stromal localisation (Figs. 2, 3, 4, 5). A similar approach was used previously for a nuclear BiFC assay where the related TagRFP was used as negative control for BiFC in the nucleus [14]. Here, we show that the FP fragment fusion to mCHERRY does not restore YFP/mVENUS fluorescence on its own (Additional file 1: Fig. S4). Furthermore, the BiFC signal we observed from the non-specific assembly of mCHERRY-nYFP and HSP21-cYFP due to high or mislocalised expression (Fig. 5, Additional file 1: Fig. S6) indicates that fusion of YFP fragments to mCHERRY does not compromise YFP re-assembly. While mCHERRY is a useful tool, we do however recommend that, where possible, a mutated version of the POI or a protein closely related to the POI is also used as a negative control because these proteins are more likely to share the same localisation and abundance as the POI [9, 14, 18, 19]. Specific interactions may also be demonstrated by the expression of a non-labelled version of the POI that competes with the FP fragment labelled version to deplete the BiFC signal [2, 18]. MoClo cloning would facilitate competition assays by allowing the straightforward addition of a transcriptional unit for an unlabelled competitor protein to the multigenic BiFC expression construct.

We found a better signal-to-noise ratio with the 174/175 YFP split [5] than with the 210/211 mVENUS split [9]. This was surprising because the mVENUS split was reported to display a particularly low level of non-specific assembly. The better performance of the 174/175 YFP split may be due to the environment of the chloroplast stroma, the specific proteins tested here, or the nature of the expression system itself. These results suggest that it may be advantageous to test more than one FP split for BiFC depending on the cellular compartment or even protein pair tested.

We investigated model stromal protein interactions in this study. In the future it would be interesting to investigate how the approach might be extended to other chloroplast compartments and to other organelles. Indeed, BiFC experiments have shown interactions between stromal proteins and integral thylakoid membrane proteins with C-terminal FP fusions [30, 49]. MoBiFC has the potential to be simply extended to other organelles such as the mitochondria, peroxisome and nucleus by the replacement of the SSU CTP modules with specific organellar targeting modules. However, care would need to be taken to avoid saturation of the import machinery and overaccumulation of the fusion proteins within the organelle as we observed here in the chloroplast under specific circumstances (Fig. 5, Additional file 1: Fig. S6). Due

(See figure on next page.)

Fig. 6 Contents of the MoBiFC kit for modular BiFC experiments. The contents of the MoBiFC kit deposited with Addgene including the Level 0 modules necessary for constructing fusion proteins for BiFC or proximity labelling, Level 1 transcriptional units including controls and reference proteins, and Level 2 multigenic constructs. The MoClo syntax for the position of different modules is indicated on the top line, and is as described by Engler et al. [6]. Modules are separated by "-", and separations within modules by "_". Full details of modules and plasmids are described in Addiitonal file 2: Table S1, S2, and full plasmid sequences are available in Additional file 4

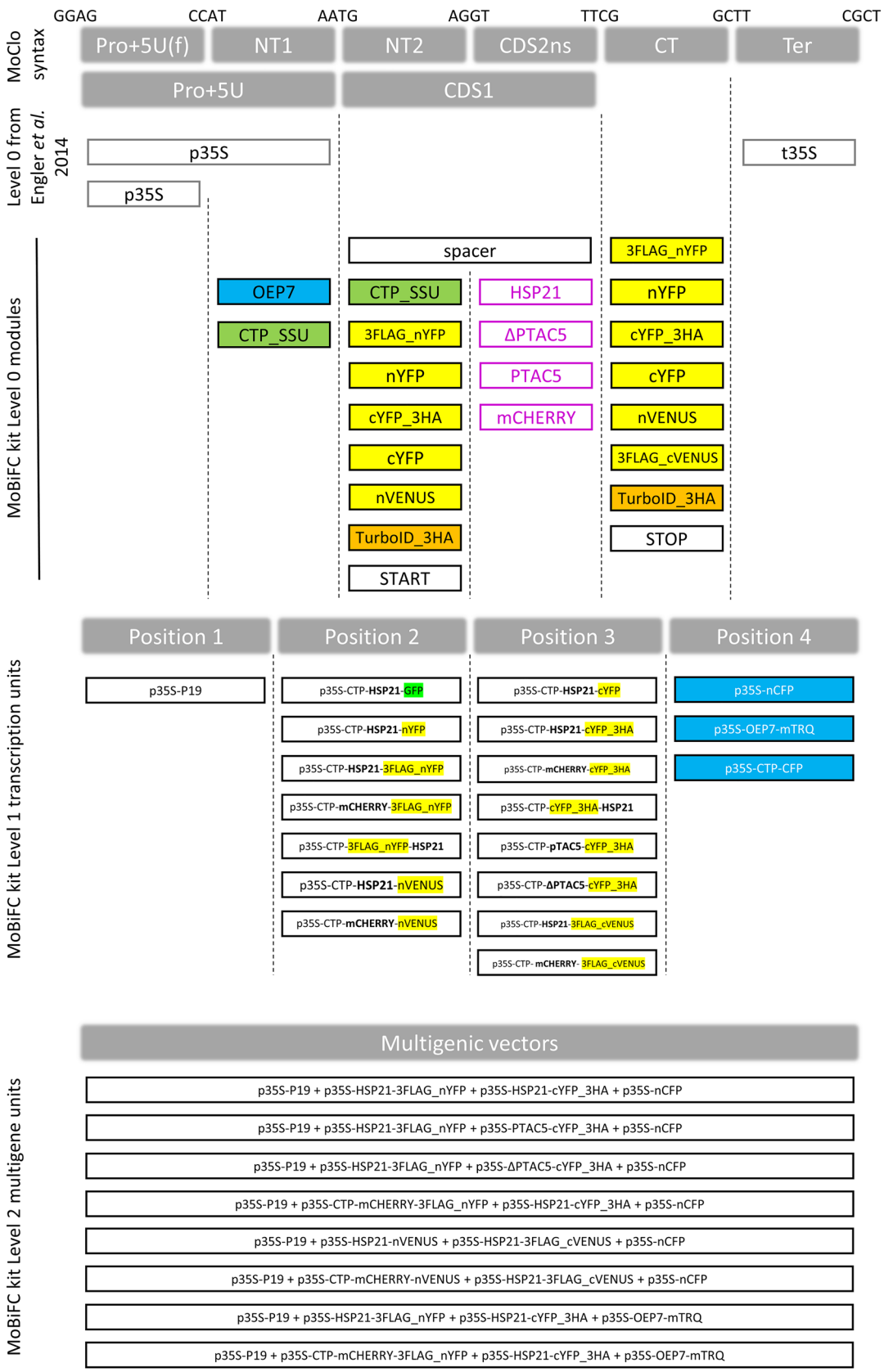

Fig. 6 (See legend on previous page.)

to its open design and the ease with which multigenic transformation constructs can be made the MoBiFC toolkit is also extendable to multicolour BiFC, the inclusion of competitor controls as discussed above, systematic high throughput library screening, and emerging techniques such as proximity labelling.

Materials and methods

Plant material and growth conditions

Nicotiana benthamiana was used for all experiments in this study unless otherwise indicated. Arabidopsis plants carrying the GVG-AvrPto transgene were used for Arabidopsis BiFC assays [47]. Both Arabidopsis and *Nicotiana* plants were grown in a controlled environment at 120 µmol m^{-2} s^{-1} illumination with an 8 h/16 h photoperiod at 22 °C day/20 °C night, and 55% day/75% night relative humidity.

Cloning

New gene parts (level 0 modules) were amplified by PCR or synthesised directly (Twist Biosciences) and sequenced. The resulting modules are free from BsaI, BsmBI, BpiI and SapI Type IIS sites and can be mobilised in the MoClo, Goldenbraid and Loop cloning systems [31, 32, 37]. Restriction ligation reactions for the assembly of transcriptional units (Level 1) and assemblies of transcriptional units (Level 2) were performed using a single step protocol as described previously with small modifications [51] and according to the MoClo Golden Gate assembly standard [6] (for detailed instructions see cloning guide in Additional file 3). Briefly, 100 fmol of each insert plasmid and 50 fmol of acceptor plasmid were mixed with restriction enzyme (BpiI or BsaI) and T4 DNA ligase in T4 ligase buffer in 20 µl reactions and incubated at 37 °C for 5 h. A 1.5 µl aliquot was transformed into DH10B cells by electroporation and transformants selected on appropriate antibiotics. Correct assembly was confirmed by digestion. Lists of new modules created and their sequences are provided in the Additional file 2: Tables S1, S2 and Additional file 4. All other Level 0 and infrastructure modules used were described previously [6, 7]. The vectors containing the principal modules for the toolkit have been deposited at Addgene (Additional file 1: Table S1).

Transient expression by agroinfiltration

Agrobacterium tumefaciens GV3101 transformed with Level 1 transcriptional units or Level 2 multigenic units were grown at 28 °C overnight in LB medium supplemented with rifampicin and a selective antibiotic. The cultures were then diluted to an OD_{600} of 0.1 in infiltration buffer containing 10 mM MES pH 5.5, 10 mM $MgCl_2$ and 200 µM acetosyringone, incubated at room temperature for 2 h and then infiltrated into leaves of one month old *N. benthamiana* plants using a 1 ml syringe. For Arabidopsis transient expression, leaves of GVG-AvrPto plants were sprayed with 2 µM dexamethasone 24 h before inoculation [47], and then infiltrated as described for *N. benthamiana*. Infiltrated plants were returned to standard growth conditions for three days before observation.

Bimolecular fluorescence complementation assays

All BiFC assays were repeated at least twice and showed similar results. Leaf discs were taken 3 days after agroinfiltration. The discs were mounted in perfluorodecalin to allow visualisation of mesophyll cells as described previously [24]. Capture of fluorescence images was performed using the AxioImager APO Z1 microscope (Zeiss). The following filters were used: chlorophyll, excitation 625–655 nm, emission 665–715 nm; mCHERRY, excitation 533–558 nm, emission 570–640 nm; YFP/mVENUS, excitation 490–510 nm, emission 520–550 nm; and CFP/mTRQ, excitation 431–441 nm, emission 460–500 nm. Standard exposure times of 5 ms for chlorophyll and 75 ms for FPs was kept for all observations. No fluorescence bleed through was observed between different FPs. Images were captured from different regions of each inoculated leaf, and from at least two leaves per experiment. 10 µm deep Z stacks composed of 21 slices were acquired and then converted into maximum intensity projections in ZEN (Zeiss). Post-acquisition image processing was then performed Image J [38, 40]. For each channel histogram levels were set identically for all images in each experiment. No oversaturated pixels were shown, except for images in Additional file 1: Figs. S2, S3 and S4 where histogram levels were modified in the same way for all images to reveal low intensity signals. For quantification of normalised fluorescence intensities unprocessed images were used, and regions of interest containing only transformed cells (i.e., those displaying reference CFP fluorescence) were defined in ImageJ. The integrated signal density was calculated for the YFP/VENUS channel in each region of interest and divided by the total chlorophyll or CFP fluorescence in the same region to provide a fluorescence intensity ratio. Graphs and statistical tests were generated in Python (Python Software Foundation, https://www.python.org/) using the Panda [28], Matplotlib [16], Seaborn [50] and Pingouin [48] packages.

Biotin labelling

Leaf discs were taken from *N. benthamiana* plants three days after agroinfiltration and infiltrated with a solution

of 50 µM biotin. After incubation for one hour under plant growth conditions discs were frozen and total proteins extracted as described below.

Immunoblotting and protein detection

Total leaf proteins were extracted in SDS sample buffer and separated by SDS-PAGE as described previously [45]. Proteins were transferred onto a nitrocellulose membrane and probed with specific antibodies. Primary antibodies targeting the HA tag (monoclonal ab9110, Abcam), FLAG tag (monoclonal 637301, BioLegend) and GFP (polyclonal A-11122, Thermofisher) were all used at a concentration of 1/3000. Biotinylated proteins were detected directly using streptavidin-horse radish peroxidase conjugate (RPN1231, Cytiva). Total proteins were visualised after separation using SYPRO ruby protein stain (Thermofisher).

Supplementary Information

The online version contains supplementary material available at https://doi.org/10.1186/s13007-022-00902-1.

Additional file 1: **Fig. S1.** Validation of 3FLAG_nYFP and 3HA_cYFP for BiFC. **Fig. S2.** Quantification of the BiFC experiments shown in Fig. 2**. Fig. S3**. Related to Fig. 4, the sensitivity of the BiFC can be adjusted with different FP splits and promoters. **Fig. S4.** mCHERRY FP fragment fusions do not show YFP fluorescence when expressed alone. **Fig. S5.** Chloroplastic CFP is unreliable as a reference FP. **Fig. S6.** Epidermal cells have a high rate of false positive signals. **Fig. S7.** BiFC in Arabidopsis. **Fig. S8.** Related to Fig. 5. OEP7-mTRQ levels are proportional to POI-nYFP levels. **Fig. S9.** Functional test of a chloroplast TurboID module.

Additional file 2: **Table S1.** List of modules in MoBiFC toolkit. **Table S2.** List of all constructs generated.

Additional file 3. MoBiFC cloning guide.

Additional file 4. Full plasmid DNA sequences for principal modules.

Acknowledgements

We thank Pascaline Auroy-Tarrago for facilitating the development of synthetic biology initiatives within the BIAM. Fluoresence microscopy experiments were performed on the PiCSL-FBI core facility.

Author contributions

FV, MS, SD, CL, PC and BF conceived and planned the experiments. FV, MS, MM, SD, PC, and BF performed the experiments. FV, MM, SD, CL, PC and BF contributed to the analysis and interpretation of the results. FV, CL, PC and BF wrote the manuscript. All authors provided critical feedback and helped shape the research, analysis, and manuscript. All authors read and approved the final manuscript.

Funding

This work was supported by Agence Nationale de la Recherche funding (G4PLAST, ANR-17-CE13-0005). MM was supported by an Erasmus international mobility Grant and a mobility grant of the University of Tunis El Manar. The PiCSL-FBI core facility is a supported by the France-BioImaging national research infrastructure (ANR-10-INBS-04).

Availability of data and materials

Vectors generated in this study can be requested from the corresponding authors. All the vectors are also available via Addgene (https://www.addgene.org).

Declarations

Ethics approval and consent to participate

Not applicable.

Consent for publication

All authors agree with submission of this version.

Competing interests

The authors declare that they have no competing interests.

Author details

[1]Aix-Marseille Univ, CEA, CNRS, BIAM, UMR7265, 13009 Marseille, France. [2]Laboratory of Molecular Genetics, Immunology and Biotechnology, Faculty of Sciences of Tunis, University of Tunis El Manar, 2092 Tunis, Tunisia. [3]Dipartimento Scienze della Vita e Biologia dei Sistemi, Università degli Studi di Torino, 10135 Torino, Italy.

Received: 17 November 2021 Accepted: 6 May 2022
Published online: 26 May 2022

References

1. Arora D, Abel NB, Liu C, Van Damme P, Yperman K, Eeckhout D, Vu LD, Wang J, Tornkvist A, Impens F, et al. Establishment of proximity-dependent biotinylation approaches in different plant model systems. Plant Cell. 2020. https://doi.org/10.1105/tpc.20.00235.
2. Bischof J, Duffraisse M, Furger E, Ajuria L, Giraud G, Vanderperre S, Paul R, Björklund M, Ahr D, Ahmed AW, et al. Generation of a versatile BiFC ORFeome library for analyzing protein–protein interactions in live *Drosophila*. Elife. 2018. https://doi.org/10.7554/eLife.38853.
3. Bracha-Drori K, Shichrur K, Katz A, Oliva M, Angelovici R, Yalovsky S, Ohad N. Detection of protein–protein interactions in plants using bimolecular fluorescence complementation. Plant J. 2004;40:419–27.
4. Branon TC, Bosch JA, Sanchez AD, Udeshi ND, Svinkina T, Carr SA, Feldman JL, Perrimon N, Ting AY. Efficient proximity labeling in living cells and organisms with TurboID. Nat Biotechnol. 2018. https://doi.org/10.1038/nbt.4201.
5. Citovsky V, Lee LY, Vyas S, Glick E, Chen MH, Vainstein A, Gafni Y, Gelvin SB, Tzfira T. Subcellular localization of interacting proteins by bimolecular fluorescence complementation in planta. J Mol Biol. 2006;362:1120–31.
6. Engler C, Youles M, Gruetzner R, Ehnert TM, Werner S, Jones JDG, Patron NJ, Marillonnet S. A golden gate modular cloning toolbox for plants. ACS Synth Biol. 2014;3:839–43.
7. Gantner J, Ordon J, Ilse T, Kretschmer C, Gruetzner R, Löfke C, Dagdas Y, Bürstenbinder K, Marillonnet S, Stuttmann J. Peripheral infrastructure vectors and an extended set of plant parts for the modular cloning system. PLoS ONE. 2018;13:1–17.
8. Goedhart J, von Stetten D, Noirclerc-Savoye M, Lelimousin M, Joosen L, Hink MA, van Weeren L, Gadella TWJ, Royant A. Structure-guided evolution of cyan fluorescent proteins towards a quantum yield of 93%. Nat Commun. 2012;3:751.
9. Gookin TE, Assmann SM. Significant reduction of BiFC non-specific assembly facilitates in planta assessment of heterotrimeric G-protein interactors. Plant J. 2014;80:553–67.
10. Grefen C, Blatt MR. A 2in1 cloning system enables ratiometric bimolecular fluorescence complementation (rBiFC). Biotechniques. 2012. https://doi.org/10.2144/000113941.
11. Grefen C, Donald N, Hashimoto K, Kudla J, Schumacher K, Blatt MR. A ubiquitin-10 promoter-based vector set for fluorescent protein tagging facilitates temporal stability and native protein distribution in transient and stable expression studies. Plant J. 2010. https://doi.org/10.1111/j.1365-313X.2010.04322.x.
12. Hecker A, Wallmeroth N, Peter S, Blatt MR, Harter K, Grefen C. Binary 2in1 vectors improve in planta (co)localization and dynamic protein interaction studies. Plant Physiol. 2015;168:776 LP – 787.

13. Hong Y, Wang Z, Liu X, Yao J, Kong X, Shi H, Zhu J-K. Two chloroplast proteins negatively regulate plant drought resistance through separate pathways. Plant Physiol. 2020;182:1007 LP – 1021.
14. Horstman A, Tonaco IAN, Boutilier K, Immink RGH. A cautionary note on the use of split-YFP/BiFC in plant protein-protein interaction studies. Int J Mol Sci. 2014. https://doi.org/10.3390/ijms15069628.
15. Hu CD, Chinenov Y, Kerppola TK. Visualization of interactions among bZIP and Rel family proteins in living cells using bimolecular fluorescence complementation. Mol Cell. 2002;9:789–98.
16. Hunter JD. Matplotlib: a 2D graphics environment. Comput Sci Eng. 2007;9:90–5.
17. Kim TW, Park CH, Hsu CC, Zhu JY, Hsiao Y, Branon T, Xu SL, Ting AY, Wang ZY. Application of TurboID-mediated proximity labeling for mapping a GSK3 kinase signaling network in *Arabidopsis*. bioRxiv. 2019. https://doi.org/10.1101/636324.
18. Kodama Y, Hu CD. Bimolecular fluorescence complementation (BiFC): a 5-year update and future perspectives. Biotechniques. 2012. https://doi.org/10.2144/000113943.
19. Kudla J, Bock R. Lighting the way to protein-protein interactions: recommendations on best practices for bimolecular fluorescence complementation analyses. Plant Cell. 2016;28:1002–8.
20. Lambert W, Koeck PJB, Ahrman E, Purhonen P, Cheng K, Elmlund D, Hebert H, Emanuelsson C. Subunit arrangement in the dodecameric chloroplast small heat shock protein Hsp21. Protein Sci. 2011;20:291–301.
21. Lampugnani ER, Wink RH, Persson S, Somssich M. The toolbox to study protein-protein interactions in plants. CRC Crit Rev Plant Sci. 2018;37:308–34.
22. Lee KH, Kim DH, Lee SW, Kim ZH, Hwang I. In vivo import experiments in protoplasts reveal the importance of the overall context but not specific amino acid residues of the transit peptide during import into chloroplasts. Mol Cells. 2002;14(3):388–97.
23. Lee YJ, Kim DH, Kim Y-W, Hwang I. Identification of a signal that distinguishes between the chloroplast outer envelope membrane and the endomembrane system in vivo. Plant Cell. 2001;13:2175 LP – 2190.
24. Littlejohn GR, Love J. A simple method for imaging arabidopsis leaves using perfluorodecalin as an infiltrative imaging medium. J Vis Exp. 2012;2:1–4.
25. Mair A, Xu SL, Branon TC, Ting AY, Bergmann DC. Proximity labeling of protein complexes and cell type specific organellar proteomes in *Arabidopsis* enabled by TurboID. Elife. 2019. https://doi.org/10.7554/eLife.47864.
26. Maple J, Aldridge C, Møller SG. Plastid division is mediated by combinatorial assembly of plastid division proteins. Plant J. 2005;43:811–23.
27. Maple J, Vojta L, Soll J, Møller SG. ARC3 is a stromal Z-ring accessory protein essential for plastid division. EMBO Rep. 2007;8:293–9.
28. McKinney W. Data structures for statistical computing in python. Proc 9th Python Sci Conf. 2010. https://doi.org/10.25080/majora-92bf1922-00a.
29. Miller KE, Kim Y, Huh WK, Park HO. Bimolecular fluorescence complementation (BiFC) analysis: advances and recent applications for genome-wide interaction studies. J Mol Biol. 2015;427:2039–55.
30. Ouyang M, Li X, Zhang J, Feng P, Pu H, Kong L, Bai Z, Rong L, Xu X, Chi W, et al. Liquid–liquid phase transition drives intra-chloroplast cargo sorting. Cell. 2020;180:1144-1159.e20.
31. Patron NJ, Orzaez D, Marillonnet S, Warzecha H, Matthewman C, Youles M, Raitskin O, Leveau A, Farré G, Rogers C, et al. Standards for plant synthetic biology: a common syntax for exchange of DNA parts. New Phytol. 2015. https://doi.org/10.1111/nph.13532.
32. Pollak B, Cerda A, Delmans M, Álamos S, Moyano T, West A, Gutiérrez RA, Patron NJ, Federici F, Haseloff J. Loop assembly: a simple and open system for recursive fabrication of DNA circuits. New Phytol. 2019. https://doi.org/10.1111/nph.15625.
33. Ramos-Vega M, Guevara-García A, Llamas E, Sánchez-León N, Olmedo-Monfil V, Vielle-Calzada JP, León P. Functional analysis of the *Arabidopsis thaliana* CHLOROPLAST BIOGENESIS 19 pentatricopeptide repeat editing protein. New Phytol. 2015;208:430–41.
34. Romei MG, Boxer SG. Split green fluorescent proteins: scope, limitations, and outlook. Annu Rev Biophys. 2019. https://doi.org/10.1146/annurev-biophys-051013-022846.
35. Rutsdottir G, Härmark J, Weide Y, Hebert H, Rasmussen MI, Wernersson S, Respondek M, Akke M, Højrup P, Koeck PJB, et al. Structural model of dodecameric heat-shock protein Hsp21: flexible N-terminal arms interact with client proteins while C-terminal tails maintain the dodecamer and chaperone activity. J Biol Chem. 2017;292:8103–21.
36. Salomon M, Fischer K, Flugge UI, Soll J. Sequence analysis and protein import studies of an outer chloroplast envelope polypeptide. Proc Natl Acad Sci USA. 1990;87:5778–82.
37. Sarrion-Perdigones A, Vazquez-Vilar M, Palací J, Castelijns B, Forment J, Ziarsolo P, Blanca J, Granell A, Orzaez D. Goldenbraid 2.0: a comprehensive DNA assembly framework for plant synthetic biology. Plant Physiol. 2013. https://doi.org/10.1104/pp.113.217661.
38. Schindelin J, Arganda-Carreras I, Frise E, Kaynig V, Longair M, Pietzsch T, Preibisch S, Rueden C, Saalfeld S, Schmid B, et al. Fiji: an open-source platform for biological-image analysis. Nat Methods. 2012. https://doi.org/10.1038/nmeth.2019.
39. Schleiff E, Tien R, Salomon M, Soll J. Lipid composition of outer leaflet of chloroplast outer envelope determines topology of OEP7. Mol Biol Cell. 2001;12:4090–102.
40. Schneider CA, Rasband WS, Eliceiri KW. NIH Image to ImageJ: 25 years of image analysis. Nat Methods. 2012. https://doi.org/10.1038/nmeth.2089.
41. Scholthof HB. The Tombusvirus-encoded P19: from irrelevance to elegance. Nat Rev Microbiol. 2006. https://doi.org/10.1038/nrmicro1395.
42. Shaner NC, Campbell RE, Steinbach PA, Giepmans BNG, Palmer AE, Tsien RY. Improved monomeric red, orange and yellow fluorescent proteins derived from *Discosoma* sp. red fluorescent protein. Nat Biotechnol. 2004;22:1567–72.
43. Shin JS, So WM, Kim SY, Noh M, Hyoung S, Yoo KS, Shin JS. CBSX3-Trxo-2 regulates ROS generation of mitochondrial complex II (succinate dehydrogenase) in *Arabidopsis*. Plant Sci. 2020;294: 110458.
44. Struk S, Jacobs A, Sánchez Martín-Fontecha E, Gevaert K, Cubas P, Goormachtig S. Exploring the protein–protein interaction landscape in plants. Plant Cell Environ. 2019. https://doi.org/10.1111/pce.13433.
45. Sugliani M, Abdelkefi H, Ke H, Bouveret E, Robaglia C, Caffarri S, Field B. An ancient bacterial signaling pathway regulates chloroplast function to influence growth and development in *Arabidopsis*. Plant Cell. 2016. https://doi.org/10.1105/tpc.16.00045.
46. Sun T, Yuan H, Chen C, Kadirjan-Kalbach DK, Mazourek M, Osteryoung KW, Li L. ORHis, a natural variant of OR, specifically interacts with plastid division factor ARC3 to regulate chromoplast number and carotenoid accumulation. Mol Plant. 2020. https://doi.org/10.1016/j.molp.2020.03.007.
47. Tsuda K, Qi Y, Nguyen LV, Bethke G, Tsuda Y, Glazebrook J, Katagiri F. An efficient *Agrobacterium*-mediated transient transformation of *Arabidopsis*. Plant J. 2012;69:713–9.
48. Vallat R. Pingouin: statistics in Python. J Open Source Softw. 2018. https://doi.org/10.21105/joss.01026.
49. Wang S, Blumwald E. Stress-induced chloroplast degradation in *Arabidopsis* is regulated via a process independent of autophagy and senescence-associated vacuoles. Plant Cell. 2014;26:4875–88.
50. Waskom M, Botvinnik O, Ostblom J, Gelbart M, Lukauskas S, Hobson P, Gemperline DC, Augspurger T, Halchenko Y, Cole JB, et al. mwaskom/seaborn: v0.10.1 (april 2020). Zenodo. 2020.
51. Weber E, Engler C, Gruetzner R, Werner S, Marillonnet S. A modular cloning system for standardized assembly of multigene constructs. PLoS ONE. 2011. https://doi.org/10.1371/journal.pone.0016765.
52. Zhang Y, Beard KFM, Swart C, Bergmann S, Krahnert I, Nikoloski Z, Graf A, George Ratcliffe R, Sweetlove LJ, Fernie AR, et al. Protein–protein interactions and metabolite channelling in the plant tricarboxylic acid cycle. Nat Commun. 2017. https://doi.org/10.1038/ncomms15212.
53. Zhang Y, Song G, Lal NK, Nagalakshmi U, Li Y, Zheng W, Huang P, Branon TC, Ting AY, Walley JW, et al. TurboID-based proximity labeling reveals that UBR7 is a regulator of N NLR immune receptor-mediated immunity. Nat Commun. 2019. https://doi.org/10.1038/s41467-019-11202-z.
54. Zhong L, Zhou W, Wang H, Ding S, Lu Q, Wen X, Peng L, Zhang L, Lu C. Chloroplast small heat shock protein HSP21 interacts with plastid nucleoid protein pTAC5 and is essential for chloroplast development in arabidopsis under heat stress. Plant Cell. 2013;25:2925–43.

Publisher's Note

Supplementary Data for Velay et al. "MoBiFC: development of a modular bimolecular fluorescence complementation toolkit for the analysis of chloroplast protein-protein interactions."

Additional File 1. Fig S1-S9

Additional file 2. Table S1-S2

Additional file 3. MoBiFC cloning guide.

Additional file 4. Full plasmid DNA sequences for principal modules.

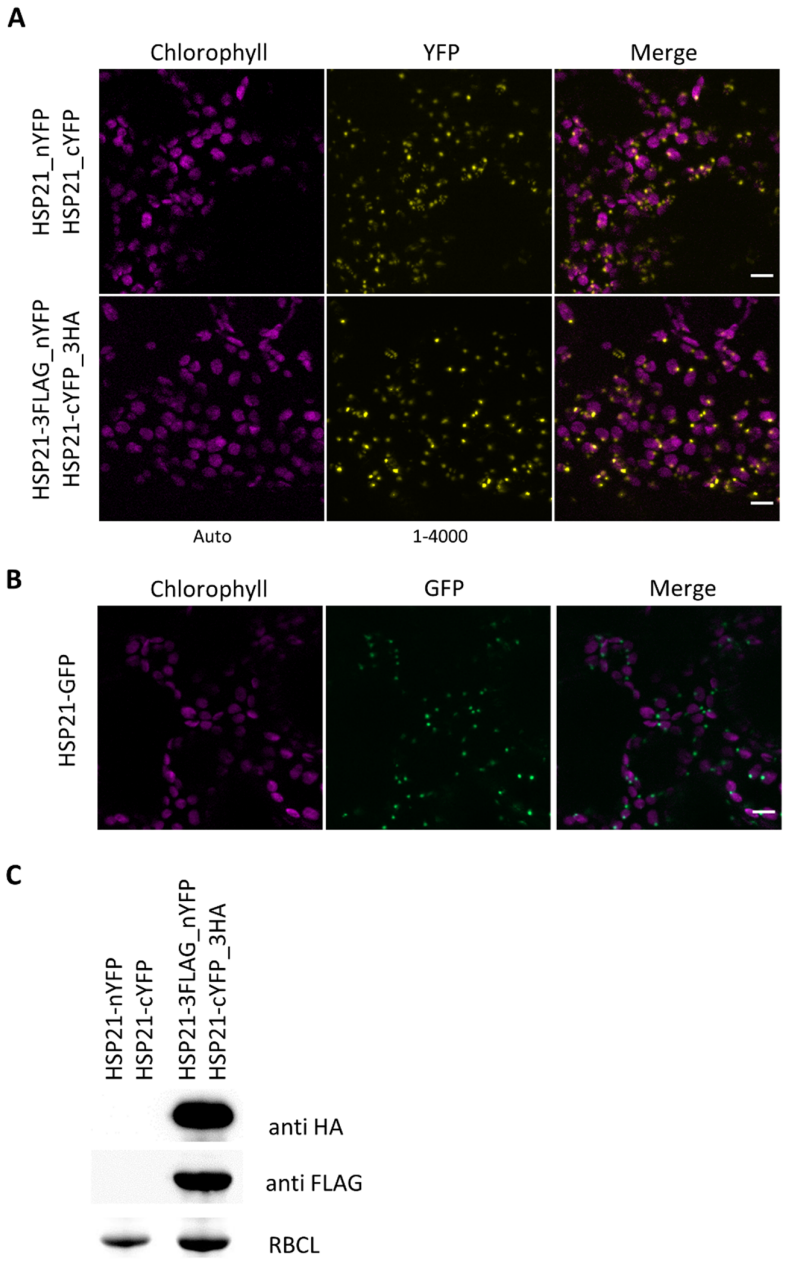

Fig. S1. Validation of 3FLAG_nYFP and cYFP_3HA for BiFC. (A) BiFC assay in *N. benthamiana* mesophyll cells showing the auto-interaction of CTP-SSU chloroplast targeted HSP21 using either untagged YFP fragments (nYFP, cYFP) or epitope-tagged YFP fragments (3FLAG_nYFP, 3HA_CYFP). Scale, 10 µm; histogram levels shown at the bottom of each channel. (B) Localisation of HSP21-GFP in *N. benthamiana* mesophyll cells. Scale, 10 µm. Standard histogram levels are indicated below each channel. (C) Immunoblots with the indicated antibodies on protein samples normalised on a weight basis from the BiFC experiment in panel A. The large subunit of Rubisco (RBCL) was visualised by Sypro fluorescent total protein stain. Modules and plasmids are described in Table S1 and full plasmid sequences are available in additional file 4.

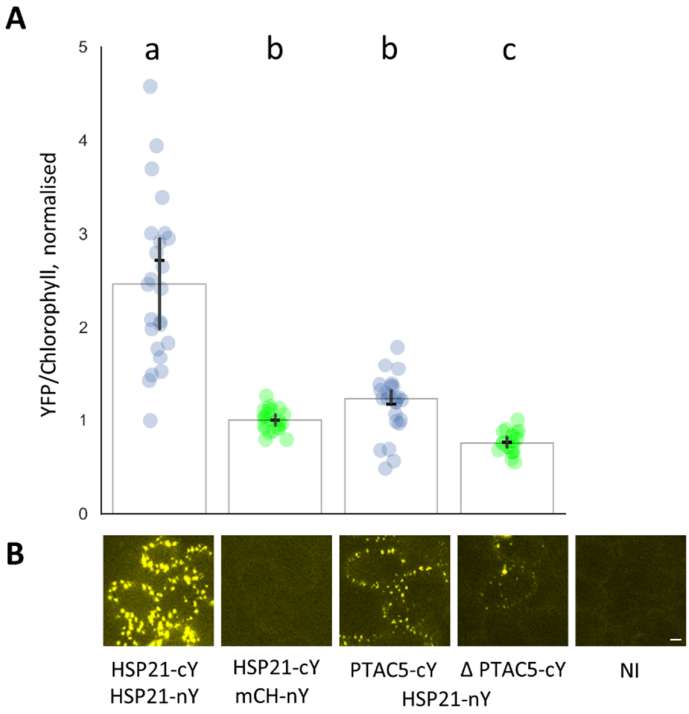

Fig. S2. Quantification of the BiFC experiments shown in Fig. 2. (A) Normalised BiFC signals were calculated as the ratio between total YFP and total chlorophyll fluorescence in transformed cells expressing CFP. The negative control HSP21-cYFP / mCHERRY-nYFP was set to 1. Horizontal line indicates mean and vertical line indicates median +/- 95% confidence interval (n=25-22 transformed cells). Significance was calculated using the Kruskal Wallis test, groups are indicated by lower case letters (*P*<0.001). (B) YFP channel images from Fig. 4 shown with a lower maximum histogram setting (i.e. saturated) to visualise low intensity signals. Please note that these images are for qualitative comparison and cannot be compared quantitatively due to the saturation. nY, nYFP; cY, cYFP; mCH, mCHERRY; NI, not innoculated.

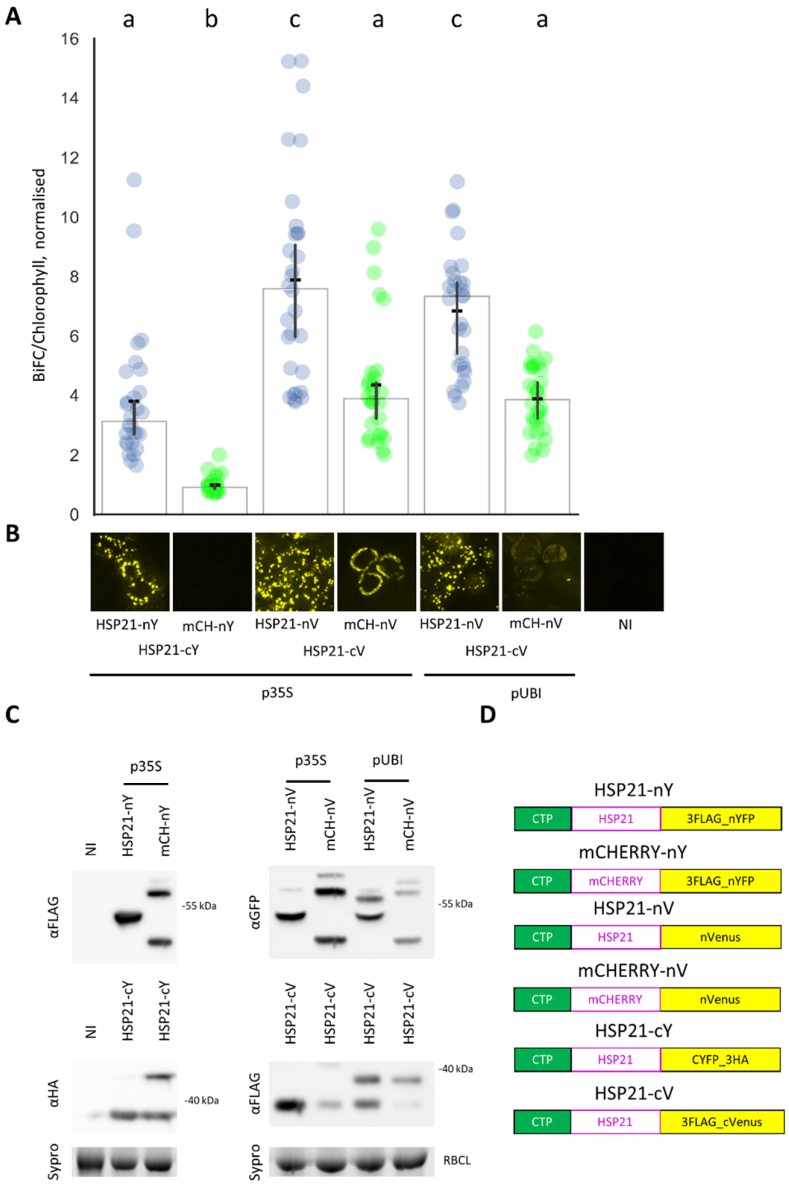

Fig. S3. Related to Fig. 4, the sensitivity of the BiFC can be adjusted with different FP splits and promoters. (A) Quantification of the BiFC experiments shown in Fig. 4. The normalised BiFC signal was calculated as the ratio between total YFP/mVENUS and chlorophyll fluorescence in transformed cells expressing CFP. The negative control HSP21-cYFP / mCHERRY-nYFP was set to 1. Horizontal lines indicate mean and vertical lines indicate median +/- 95% confidence interval (n=28-30 transformed cells). Significance was calculated using the Kruskal Wallis test, groups are indicated by lower case letters (P<0.001). (B) BiFC signal from Fig. 4 shown with a lower maximum histogram setting (i.e saturated) to visualise background signal present in HSP21-cVENUS / mCherry-nVENUS experiments. Please note that these images are for qualitative comparison and cannot be compared quantitatively due to the saturation. (C) Immunoblots with the indicated antibodies on protein samples normalised on a fresh-weight basis from the BiFC experiments in Fig. 4. Detected proteins are indicated above each blot, and sample order corresponds to order in panels A and B. The large subunit of Rubisco (RBCL) was visualised by Sypro fluorescent total protein stain. (D) Summary of proteins detected in panel C. anti-FLAG recognises the FLAG tag in 3FLAG_nYFP (nY) and 3FLAG_cVENUS (cV); anti-GFP recognises 3FLAG_nYFP (nY) and nVENUS (nV); and anti-HA recognises 3HA_cYFP (cY). The large subunit of Rubisco (RBCL) was visualised by Sypro fluorescent total protein stain. mCH, mCHERRY; NI, not innoculated.

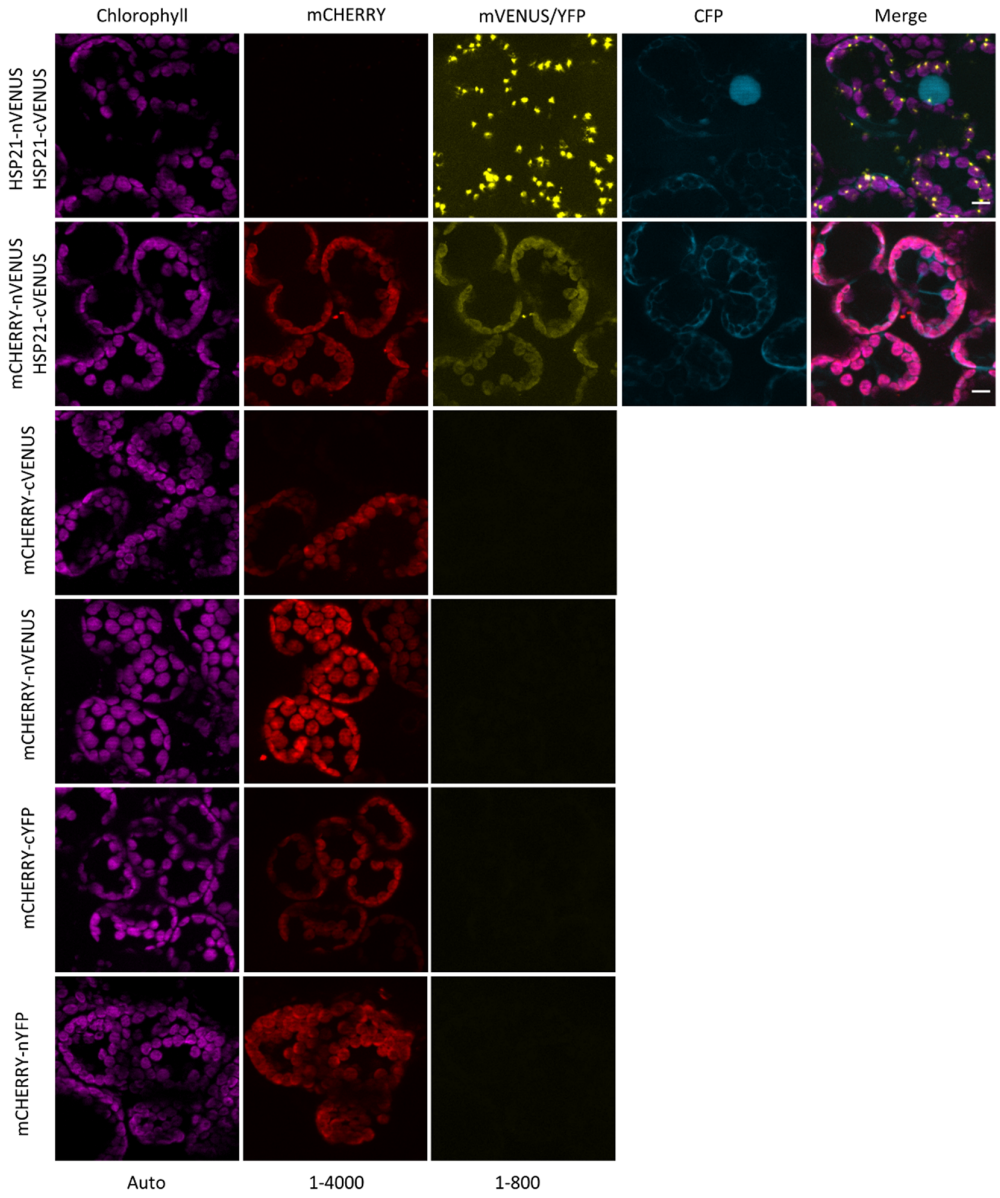

Fig. S4. mCHERRY FP fragment fusions do not show YFP fluorescence when expressed alone. BiFC signals in *N. benthamiana* epidermal cells with the indicated proteins. Scale, 10 µm. Modules and plasmids are described in Table S1 and full plasmid sequences are available in additional file 4.

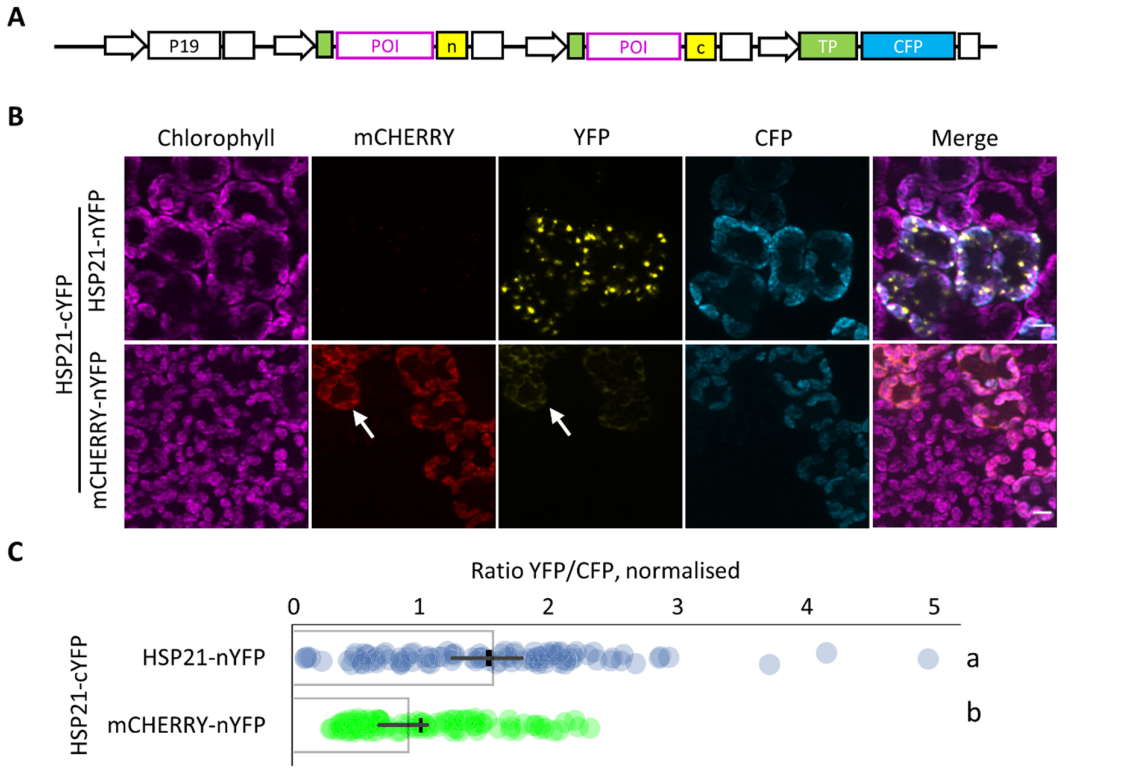

Fig. S5. Chloroplastic CFP is unreliable as a reference FP. (A) Two different HSP21 pairs with the chloroplastic CFP reference FP were used for (B) BiFC assays in *N. benthamiana* mesophyll cells. Scale, 10 µm. Arrows indicate cytosolic signal. (C) Normalised BiFC signals were calculated as the ratio between total YFP and CFP fluorescence. The negative control HSP21-cYFP / mCHERRY-nYFP was set to 1. Vertical line indicates mean and horizontal line indicates median +/- 95% confidence interval (n=100 transformed cells). Significance was calculated using the Kruskal Wallis test, groups are indicated by lower case letters (P<0.01). Modules and plasmids are described in Table S1 and full plasmid sequences are available in additional file 4.

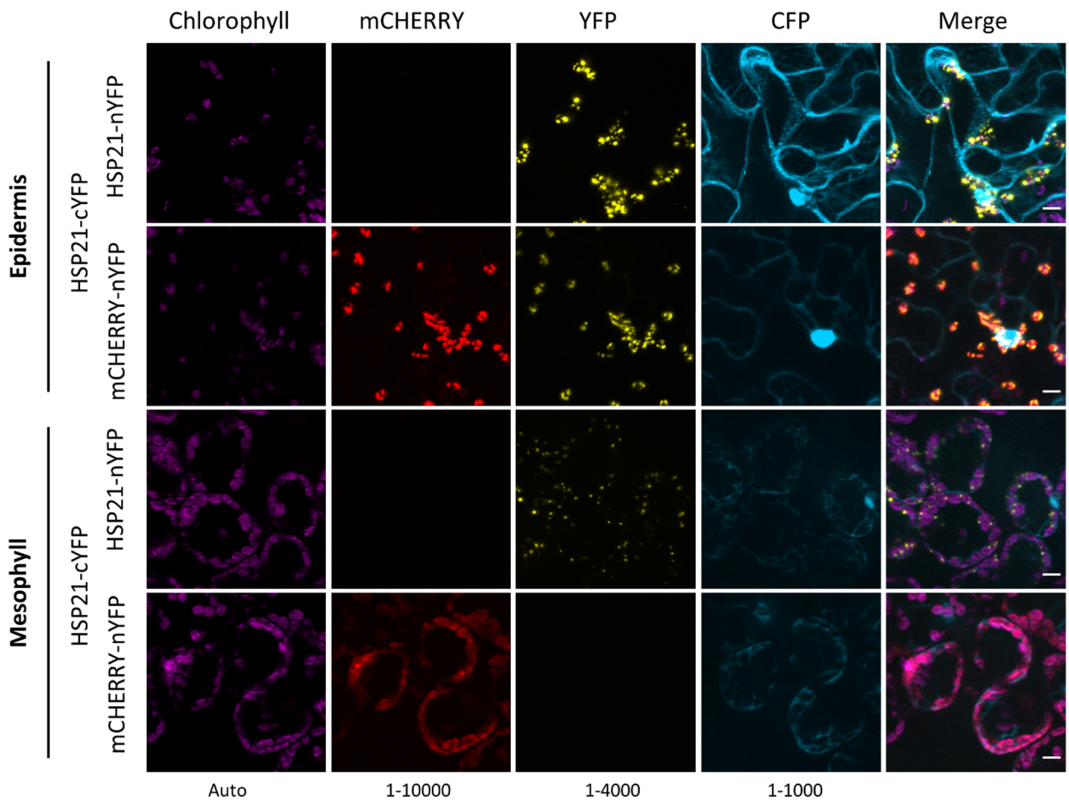

Fig. S6. Epidermal cells have a high rate of false positive signals. HSP21-HSP21 and mCHERRY-HSP21 BiFC assays in *N. benthamiana* epidermal cells (upper two rows) and mesophyll cells (lower two rows). Mesophyll images are of the same region as shown in Fig. 2. Scale, 10 μm.

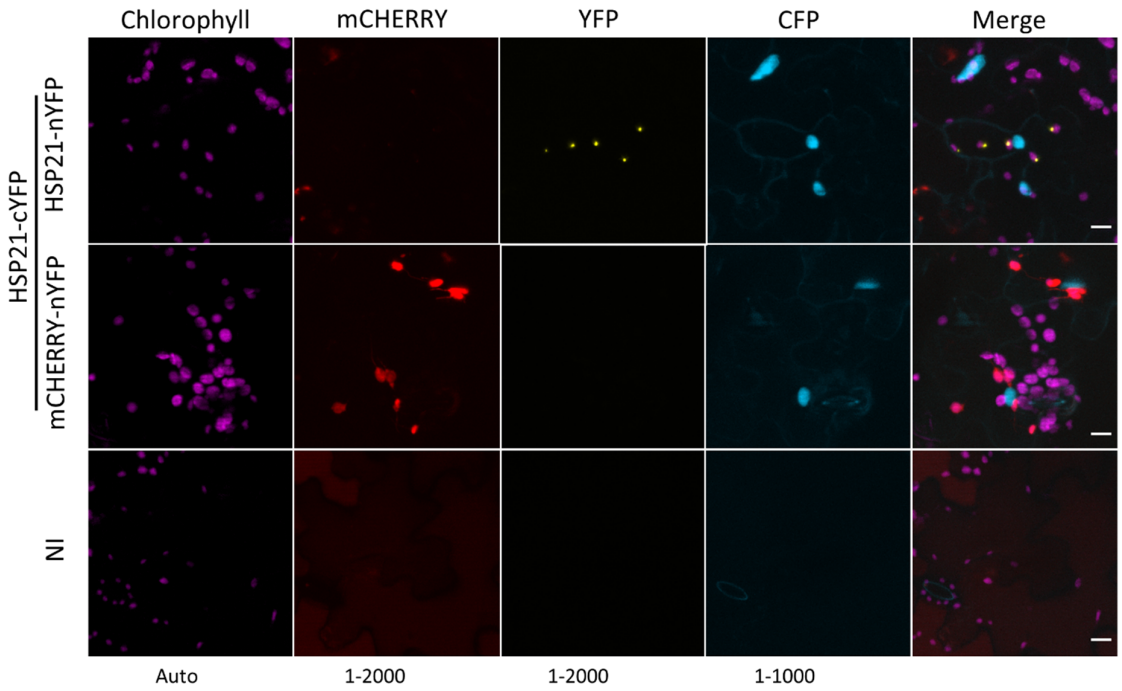

Fig. S7. BiFC in Arabidopsis. HSP21-HSP21 and mCHERRY-HSP21 BiFC assays in *A. thaliana* epidermal cells. No transformed cells were detected in the mesophyll. NI, not inoculated; scale, 10 µm.

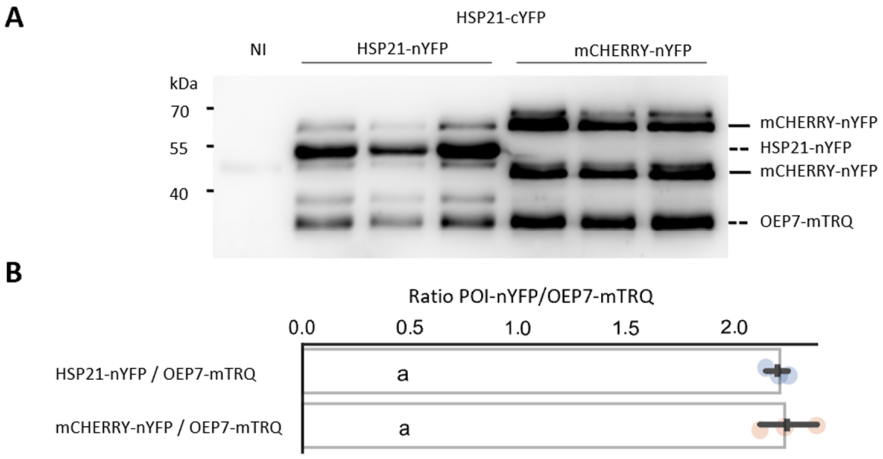

Fig. S8. Related to Fig. 5. OEP7-mTRQ levels are proportional to POI-nYFP levels. (A) Immunoblot with anti-GFP equal quantities of protein from three biological replicates of the two BiFC experiments described in Fig. 5. Detected proteins are indicated to the right, note that anti-GFP recognises mTRQ and nYFP. The large subunit of Rubisco (RBCL) was visualised by Sypro fluorescent total protein stain. (B) Quantification of the ratio between the POI-nYFP and OEP7-mTRQ. Vertical line indicates mean and horizontal line indicates median +/- 95% confidence interval. Significance was calculated using the Kruskal Wallis test, groups are indicated by lower case letters. No significant difference was observed.

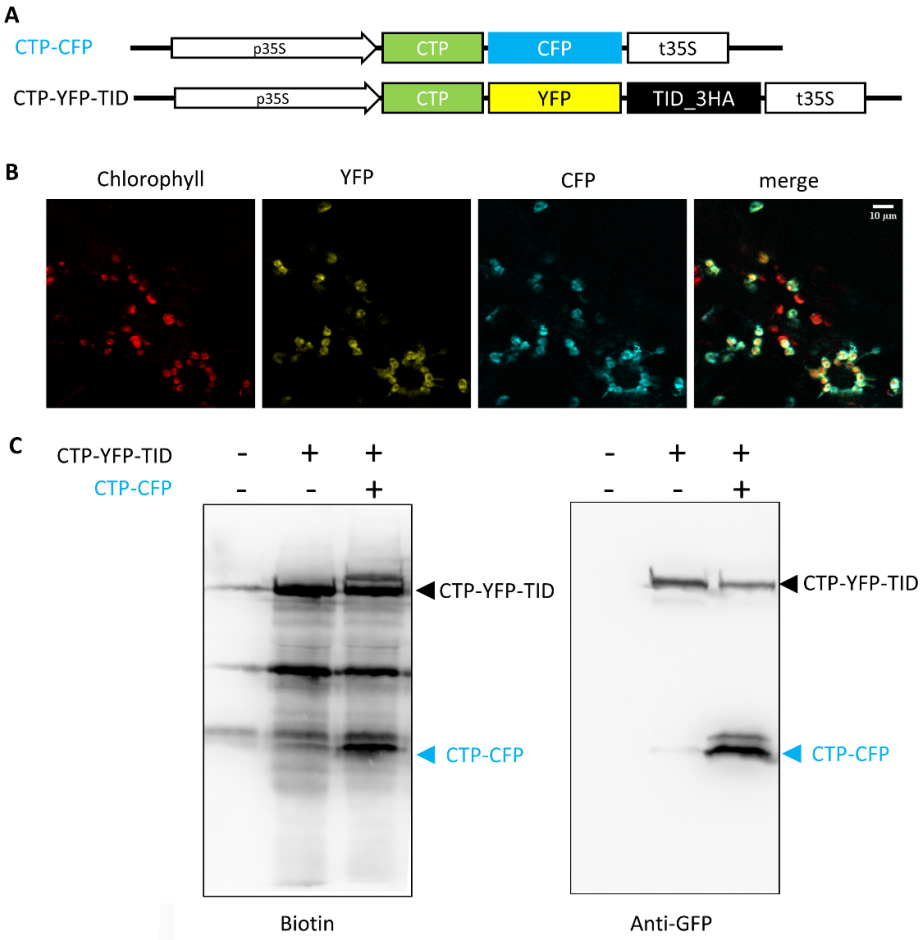

Fig. S9. Functional test of a chloroplast TurboID module. (A) Level 1 modules assembled for testing TurboID (TID). (B) Localisation of CTP-YFP-TID and CTP-CFP in the chloroplasts of co-inoculated *N. benthamiana*. Scale, 10 µm. (C) Detection of biotinylated proteins using streptavidin coupled to horse radish peroxidase and CFP/YFP using anti-GFP antibodies in total protein extracts. Leaf discs from non-inoculated plants, plants inoculated with CTP-YFP-TID only and CTP-YFP-TID + CTP-CFP were incubated with biotin for 1 hr before protein extraction, separation and detection. Biotinylation of the chloroplast localised CFP (CTP-CFP) was observed. Modules and plasmids are described in Table S1 and full plasmid sequences are available in additional file 4.